MULTISCALE FLUID DYNAMICS IN POROUS MEDIA: APPLICATIONS IN ENHANCED OIL RECOVERY

Vladivostok F. Suxo M.

Caetano R. Miranda

fsuxo@usp.br

cmiranda@if.usp.br

Department of Mechanics and Materials Physics, Institute of Physics, University of São Paulo

Rua do Matão, Travessa R, Nr. 187, Butantã, 05508090, Cidade Universitária, São Paulo, Brazil

Abstract. *The understanding of the adsorption and wettability in rock-brine-oil interfaces is crucial to estimate the amount of crude oil that can be potentially extracted from natural reservoirs. One of the most promising applications of nanotechnology in Oil & Gas industry, it is the potential of nanostructures as wettability modifiers for Enhanced Oil Recovery (EOR) processes. These nanostructures can be produced economically feasible in large scale with a certain degree of control and stable at reservoir conditions. In addition, their surface and interfacial properties can be tuned for a given geological reservoir. For EOR processes, it is also important to characterize the fluid flow and porous media (mineralogy and morphology) by considering the connectivity, porosity, tortuosity and permeability. In this work, we apply a hierarchical multi-scalar calculation protocol to explore the potential applications of the intelligent nanofluids for EOR processes. In this multiscale approach, the thermodynamics and transport properties are obtained through Molecular Dynamics (MD) and then mapped as Lattice Boltzmann Method (LBM) parameters. Our objective is two-fold: i) to quantify the porosity versus permeability relation for different pore geometry and size distribution and ii) determine how a given nanoparticle (NP) dispersion can effectivelly displace oil. More specifically, we study the injection of NP dispersion in montmorillonite (MMT) clay pore structures, previously filled by oil. Distinct functionalized SiO_2 NPs have been considered (hydroxylated, sulfonic acid, and polyethyleneglycol) dispersed in brine (API:* 8% *NaCl and* 2% *$CaCl_2$). In addition, this displacement process is studied in porous media that have the same porosity but different geometric configurations, varying: form (squares, hexagons, octogons and circles), size (circles of four different ratio) and pore distribution (four configurations). Our results indicate that for a given porosity and same injected fluid, more oil is displaced for squared shapes and small circles. While, for the same geometry, the PEGylated NP dispersed fluid are more effective to displace oil with respect to the other NPs and the brine injections.*

Keywords: *Enhanced Oil Recovery, Lattice Boltzmann Method, Molecular Dynamics, Microfluidics, Nanoparticles*

INTRODUCTION

Nowadays, there is a significant research effort to optimize and develop new oil recovery processes from natural reservoirs. In average, 5 to 25% of the total oil in the reservoir can be recovered by natural depletion, whereas, 10 to 20% additional oil may be extracted by water flooding or gas injection. The target of these new methods is to recover the remaining fraction which is mainly associated with oil trapped in the rock porous media through capillarity forces and interfacial phenomena. In this context, understanding the rock-oil-brine wettability mechanism is of primary importance to estimate the amount of potential crude oil that could be recovery from underground resources (Morrow et al., 1990; Green et al., 1998; Starov et al., 2007; Donaldson et al., 2008).

In this direction, one of the most promising applications of nanotechnology in oil & gas industry is the potential use of nanostructures as wettability modifiers for EOR processes (Suleimanov et al., 2011). These nanostructures can be economically feasible to be produced in large scale with a certain degree of control. Also, these NPs can stable at reservoir conditions and their surface and interfacial properties can be tuned for a given geological reservoir (Munshi et al., 2008). For EOR processes, it is also important to characterize the behavior of injected NPs dispersed fluid flow by taking in account the connectivity, porosity, tortuosity and permeability through a rock porous media (mineralogy and morphology).

From MD simulations we can obtain: the interfacial tension between the fluids in contact (displaced and injected) and wettability involving the fluids and the fluids and the porous matrix (digital rocks). This information obtained at the nanoscale is introduced into the microscale field, where they are treated as microscopic interactions: fluid-fluid and fluid-solid within the lattice Boltzmann method. The physical observables obtained from the microscale (density and velocity of the fluids) can be compared with the macroscopic variables of hydrodynamics applied to microfluids.

In this context, computational fluid dynamics (CFDs) can play an important role. In particular, the LBM, given its simplicity to model the dynamics, the easy handling of complex geometries and especially its flexibility for implementation in parallel computing. LBM was first derived by McNamara and Zanetti et al. 1988, since then, it has emerged as an alternative powerful method for solving CFD problems. It was very successful to simulate complex flows, such as: fluids with immiscible components, interfacial problems, fluid flow in penetrable media, fluid simulations of multiples species and flows in fairly complex porous media (Porter et al., 2012). In recent years, LBM has been extended even to semiclassical (Rodrigo et al., 2016) and relativistic fluids (Mendoza et al., 2010). Here, we will characterize the petrophysics properties of injected NPs dispersed fluid flow through artificial rock porous media with controlled geometries by using an hierarchical approach which combines LBM and MD simulations (Pereira et al., 2016).

METHODOLOGY

The computer simulation of the EOR is performed mainly from the LBM using the software TAXILA (Coon et al., 2014), with the purpose of estimating the recovery factor of a solution with chemical additives injected on matrices of different materials and geometries filled with petroleum or gas or other fluid of interest. The physicochemical characteristics of the system

(pore matrix and fluid): density, viscosity, surface tension and wettability were previously determined by Molecular Dynamics calculations (Miranda et al. 2012; de Lara et al. 2012a; Pereira et al., 2016) using the LAMMPS software (Plimpton et al. 1995).

Our previous MD simulations (Miranda et al., 2012; de Lara et al., 2012a; de Lara et al., 2012b; Rigo et al., 2014; Sánchez et al., 2014; Pereira et al., 2016; Alvim et al., 2017), indicate that the addition of SiO_2 nanoparticles to the brine solutions reduces the interfacial tension between brine and oil, followed by an increase of the contact angle between clay and oil. In order to investigate how these interfacial properties changes will affect the oil recovery process in porous network models (PNM) that emulate real pores, LBM simulations are used to determine the effects of SiO_2 nanoparticles within oil extraction process. The study of the oil extraction process in a basic pore structure, shows that the observed reduction of the interfacial tension and the increase of the contact angle by the inclusion of nanoparticles, leads to a considerable amount of oil displacement, thus, enhancing the oil recovery.

The results generated at the nanoscale are mapped as parameters in Boltzmann method simulations to explore the oil extraction process at the microscale (Pereira et al., 2016; Alvim et al., 2017). For the microscale simulations, the fluid-flow is modeled within the explicit forcing LBM (Porter et al., 2012), which is a multicomponent interparticle-potential LBM for immiscible fluids with large viscosity ratios, where the external forces are directly incorporated into the discrete Boltzmann equation. TAXILA development by Coon et al., 2014, is an open-source to solve the LBM that incorporates external forces directly and is written in Fortran, C++ and Python. Built with MPI instructions, a standard for message-based parallelism, TAXILA uses PETSc to abstract data structures and communications, which, enables codes to achieve excellent parallel performance.

Molecular Dynamics

Our group at IFUSP has applied classical molecular dynamics to determine interfacial and structural properties of NPs in oil-brine-rock interfaces at nanoscale (Miranda et al. 2012; de Lara et al. 2012a, Pereira et al., 2016). All relevant systems have been fully atomistically taken in account: clay, brine, oil and various types of nanoparticles. In particular, in these calculations, MMT clay interacts with $i)$ an API brine solution (8% NaCl and 2% $CaCl_2$) and three types of SiO_2 nanoparticle solutions: $ii)$ hydroxylated (NP-H), $iii)$ functionalized with sulfonic acid (NP-SA) and $iv)$ functionalized with polyethylene glycol (NP-PEG2).

Given that the MD calculations on these systems at the relevant thermodynamic conditions for the properties of interest are already published (Miranda et al., 2012; de Lara et al., 2012a; Pereira et al., 2016), here no further MD calculation was needed. In these published MD studies on nanoparticles within API brine-oil interface confined between montmorillonite (MMT) slits, the potentials used in the interactions of the clay-brine-oil system and nanoparticles, are: $i)$ CLAYFF potential (Cygan et al., 2004) for MMT, $ii)$ SPCE/FH potential (Alejandre et al., 2009) for API brine, $iii)$ CHARMM potential (Brooks et al., 2009) for light oil and $iv)$ CHARMM potential based in Cruz-Chu et al., 2006, for SO_2 nanoparticle. In these studies, the averaged density, viscosity, interfacial tension, and the contact angle were determined over a $4\,ns$ simulation within the NVT (number of particles, Volume and Temperature constant) ensemble after the system equilibration (See, Tab. 1).

Table 1: Summary of the molecular dynamics results for density (ρ), kinetic viscosity (ν), interfacial tension (γ) and contact angle (θ) at $1\,atm$ and $300\,°K$

System	Brine		Oil		Brine-Oil	
	$\rho_b\ (Kg/m^3)$	$\nu_b\ (10^{-6}m^2/s)$	$\rho_o\ (Kg/m^3)$	$\nu_o\ (10^{-6}m^2/s)$	$\gamma_{bo}\ (Kg/s^2)$	$\theta_w\ (\ ^\circ)$
no-NP	997	0.791	810	4.473	0.043	21
NP-H	1026	0.867	810	4.348	0.038	26
NP-SA	1037	0.867	810	4.395	0.033	33
NP-PEG2	1034	0.854	810	4.384	0.029	40

Lattice Boltzmann method

The LBM method is based on the Boltzmann theory, which describes the behavior of a system by the distribution of a set of (fictitious) particles, where, the discretization of the Boltzmann kinetic equation generates a discrete domain called lattice, in which the particles are confined (Sukop et al., 2007). The discretized kinetic models can be used because the fluid dynamics is the result of the collective behavior of many microscopic particles in the system (Succi et al., 2001). In this method, the dynamics of a fluid mixture is represented by a set of particle distribution functions on a discrete two or three dimensional lattice (Mohamad et al., 2011). The properties of the particles that interact with one another in a position k of the physical space, is represented by a distribution function:

$$f^k_{i(\boldsymbol{x}+\boldsymbol{e}_i\Delta t,t+\Delta t)} - f^k_{i(\boldsymbol{x},t)} = \frac{1}{\tau_k}\left[f^{eq,k}_{i(\boldsymbol{x},t)} - f^k_{i(\boldsymbol{x},t)} - \frac{\Delta t}{2} f^{F,k}_i\right] + \Delta t\, f^{F,k}_i \tag{1}$$

where, τ_k is the dimensionless relaxation time for each fluid component k, which is related to the kinematic viscosity by $\nu_k = (\tau_k - 0.5)/3$. The equilibrium particle distribution function $f^{eq,k}_i$, forcing terms $f^{F,k}_i$, and velocity vectors $\boldsymbol{e}_i$ has the same form as implemented by Porter et al., 2012. The forcing terms are able to reproduce distinct physical effects, including external body forces, internal forces such as inter-particle potentials (surface tension), and cohesive forces to solid surface (fluid wettability).

Interparticle potential forces, enable phase separation and surface tension to be included easily in the LBM.

$$\boldsymbol{F}^k_{ff} = -\rho_{k(\boldsymbol{x})} \sum_{k'=1}^{n_k} \sum_{x'\in\mathcal{N}_x} \mathcal{G}_{k,k'(|\boldsymbol{x'}-\boldsymbol{x}|)} \frac{\rho_{k(\boldsymbol{x'})} - \rho_{k(\boldsymbol{x})}}{|\boldsymbol{x'}-\boldsymbol{x}|}(\boldsymbol{x'}-\boldsymbol{x}) \tag{2}$$

where, the second summation is taken over a set of lattice sites $\mathcal{N}_x$ which do not include wall, and $\mathcal{G}_{kk'} = \mathrm{g}_{kk'}\tilde{\mathcal{G}}$ where $\mathrm{g}_{kk'}$ specifies the strength of forces and equivalently the surface tension, while $\tilde{\mathcal{G}}$ enforces isotropy and spatial extent that increases the numerical stability and allows the simulation of fluid mixtures with high viscosity ratios. Such fluid-fluid forces enable phase

separation and surface tension to be easily included in LBM. As presented by Porter et al., 2012, there is a unique relationship between the surface tension and the interaction strength g_{12} of a binary mixture, which is independent of the chosen viscosity and viscosity ratio. They have shown that, a simple quadratic fit ($\tilde{\gamma}_{12} = -1.361\,\mathrm{g}_{12}^2 + 1.721\,\mathrm{g}_{12} - 0.178$) can be used to estimate the surface tension $\tilde{\gamma}_{12}$ of a given binary mixture of any viscosity and viscosity ratio.

Cohesive forces to solid geometry are included through a force fluid-solid of the following form:

$$\boldsymbol{F}_{fs}^{k} = -\rho_{k(\boldsymbol{x})} \sum_{m=1}^{n_s} \mathrm{g}_k^s \sum_{x' \in \mathcal{W}_s} (\boldsymbol{x'} - \boldsymbol{x}) \tag{3}$$

where, g_k^s indicates fluid component k's affinity for mineral m and $\mathcal{W}_s$ indicates the set of neighboring sites $\boldsymbol{x} + \boldsymbol{e}_i$ which represent a wall node of mineral m. In multicomponent or multiphase simulations, this yields a contact angle, where positive g_k^s indicates a non-wetting fluid and negative g_k^s indicates a wetting fluid.

The macroscopic properties for density, momentum and pressure of each fluid component (physical observables) are defined as follows (Mohamad et al., 2011; Porter et al., 2012):

$$\rho_k = \sum_i f_i^k \tag{4}$$

$$\rho_k \boldsymbol{u}_k = \sum_i f_i^k \boldsymbol{e}_i \tag{5}$$

$$p_k = \frac{1}{3} \sum_k \rho_k + 3 \sum_{kk'} \mathrm{g}_{kk'} \rho_k \rho_{k'} \tag{6}$$

The above LBM equations are in lattice units, and a relation with the physical units can be stabilished via a characteristic scale (l_o, t_o, m_o). This characteristic scale can be easily estabilished by defining the dimensionless conversion from a physical parameter to a computational LBM parameter. This characteristic scale can be easily estabilished by defining the dimensionless conversion from a physical parameter to a computational LBM parameter. Initialy, we define three computational parameters, namely, lattice size $\tilde{L}_x$, oil density $\tilde{\rho}_o$ (or brine density $\tilde{\rho}_b$) and the interfacial tension between oil and brine $\tilde{\gamma}_{ob}$. This way, the characteristic scale can be determined as follows (Pereira et al., 2016):

$$L_x = l_o\, \tilde{L}_x \qquad \longrightarrow \qquad l_o = \frac{L_x}{\tilde{L}_x} \tag{7}$$

$$\rho_o = \frac{m_o}{l_o^3}\, \tilde{\rho}_o \qquad \longrightarrow \qquad m_o = \frac{\rho_o}{\tilde{\rho}_o}\, l_o^3 \tag{8}$$

$$\gamma_{bo} = \frac{m_o}{t_o^2}\,\tilde{\gamma}_{bo} \qquad \longrightarrow \qquad t_o = \sqrt{\frac{\tilde{\gamma}_{bo}}{\gamma_{bo}}\,m_o} \tag{9}$$

For a successful simulation, you must have a set of consistent and valid lattice parameters. The analysis of convergence and stability of solutions, especially solutions that do not violate physical principles, must be done through the criteria (Inamuro et al., 1997; Gan et al., 2008; Yang et al., 2012): Reynolds number, Mach number and Knudsen number.

$$R_e = \frac{UL}{\nu} \tag{10}$$

$$M_a = \frac{U}{c_s} \tag{11}$$

$$K_n = \frac{M_a}{R_e} \tag{12}$$

where, L and U are the characteristic length and velocity of the system (example, width of the porous media and velocity injection respectively), ν is the kinematic viscosity of a fluid in interest (in this case, with respect to oil) and c_s is the velocity of sound.

Fluid flow in porous media

One of the key issues in the physics of porous media is to describe the flow delay by the porous media network, also, how it correlates with the porous geometry and morphology. The most relevant quantities related to fluid dynamics in porous media are: porosity, tortuosity, surface area and permeability. Below, we define them as it has been used in this work:

a) Porosity (ϕ) is defined as the fraction between the total volume that is occupied by connected pores V_{pores} and total volume of the porous medium V_{total} (Scheidegger et al., 1974), as show on Eq. 13:

$$\phi = \frac{V_{pores}}{V_{total}} \tag{13}$$

The media with non-connected pores do not allow flow, therefore, do not need to be considered for our purposes. In the models studied, the medium has both connected and non-connected pores, where the volume occupied by the latter must be disregarded.

b) Tortuosity (τ) is a geometrical figure-of-merit that indicates how much the fluid flow streamlines deviate from straight paths. It is defined as the ratio between the total length, L_{stream}, along the streamline and its effective length, L_{effect}, the length of the straight line connecting final and initial position (Scheidegger et al., 1974), as it show on Eq. 14:

$$\tau = \frac{L_{stream}}{L_{effect}} \tag{14}$$

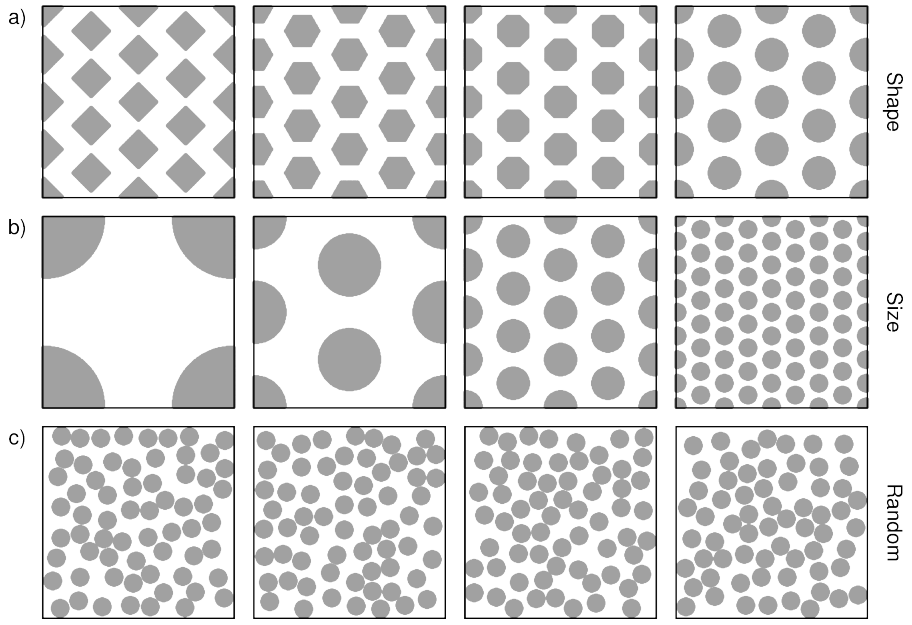

Figure 1: Basic pore structures that have the same porosity, used in our simulations. Gray regions represent solid area, while the white color stands for pore space. Structures are classified into three types, according to the solid region: a) different shapes, b) different sizes and c) random distribution.

This definition of tortuosity is essentially geometric and may bring some difficulties when applied to porous media. Alternatively, we use concept of hydraulic tortuosity (Duda et al., 2011) expressed as follows:

$$\tau = \frac{\sum_r \boldsymbol{v}_{(\boldsymbol{r})}}{\sum_r \boldsymbol{v}_{x(\boldsymbol{r})}} \tag{15}$$

where r run through all nodes of the network, therefore, $\boldsymbol{v}$ is the velocity of each point of the system and $\boldsymbol{v}_x$ is its component along the direction of the flow.

Case studies

In this work, we explore the role $i)$ of PNM in 2D and $ii)$ the effects of NP's within EOR processes at microscale. Regarding the effect of the porous structure (see, Fig. 1), three cases were considered: $a)$ different shapes, $b)$ size variation and $c)$ random distributions. Where, for each situation, four different pores are compared. The porosity was kept constant for all cases studied. For the injected fluid, four cases are taken in account (see, Tab. 1) for the same porous structures. First, only the API brine injection, then, three types of nanoparticle solutions are individually included: NP-H, NP-SA and NP-PEG2.

Initially, the petrophysics properties of the PNM are characterized, such as: porosity through Eq. 13 and its respective tortuosity, through Eq. 15. In the latter case, the hydraulic tortuosity is obtained. To apply Eq. 15, it is necessary that the velocity field of the fluid reach at a stationary state. To perform a test to the applied methodology, we proceed to obtain the hydraulic tortuosity of the system of Fig. 2. This system consists of a channel at different angles of inclination (in this case, only four angles), with respect to the horizontal line, where, the geometrical tortuosity of this system is well known (Duda et al., 2011) and has the following analytical solution:

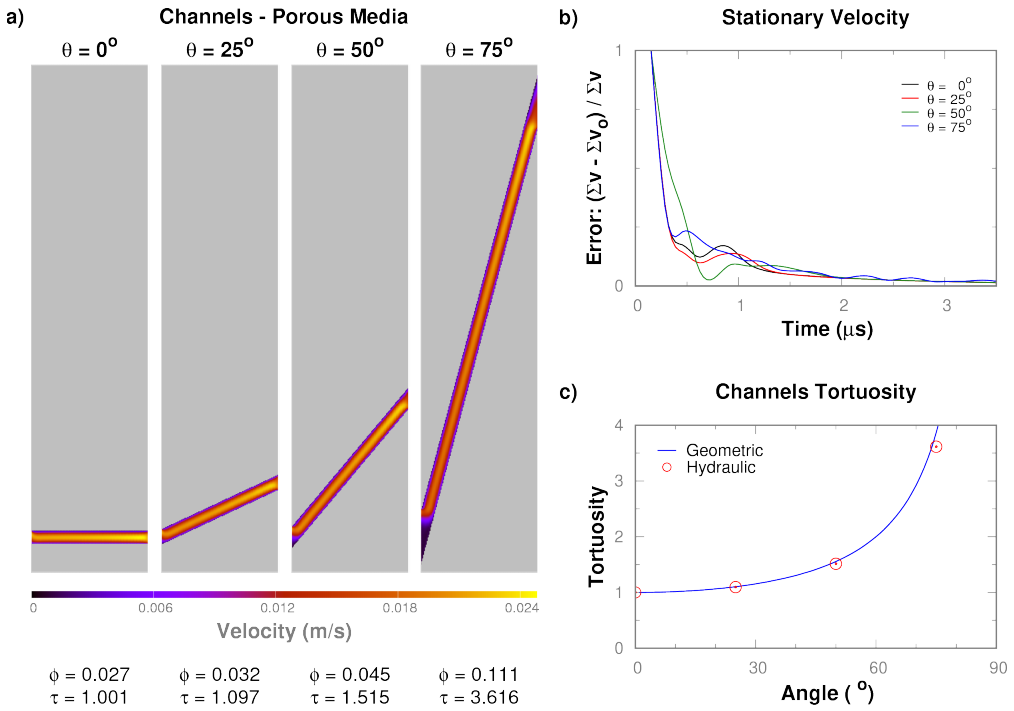

Figure 2: Tortuosity in a channel with constant width at different angles. a) Fluid velocity in the channels, yellow color is maximum velocity and black color is zero velocity. b) Stationary velocity in the channels reached in a short time. c) Comparison between geometric tortuosity and hydraulic tortuosity.

$$\tau = \frac{1}{\cos\theta} \tag{16}$$

The hydraulic tortuosity was obtained only for four angles of inclination (see, Fig. $2a$), when the system reaches a stationary state. This occours at approximately $3\,\mu s$ in the four cases, as shown in Fig. $2b$. Finally, in Fig. $2c$, we can see the results obtained in comparison with the analytical solution (Eq. 16). This suggests that hydraulic tortuosity method is valid.

RESULTS

All the studied porous structures are square regions, with dimensions of $5.68 \times 5.68\,\mu m$ ($L_x \times L_y$), each one with a different pore configuration, as show on Fig. 1. All the structures are designed to have the same porosity $\phi = 0.69$ (Eq. 13), while, the tortuosity is obtained by the hydraulic technique and the result is constant for all the structures $\tau = 1.12$ (Eq. 15). To displace the oil that initially occupies the entire porous structure, is injected brine (with or without Np's) with a velocity of $v = 0.44\,m/s$ from left to right in all cases.

In order to explore how $i)$ the structure of the PNM and $ii)$ the addition of SiO_2 nanoparticles to the brine solution will affect the oil displacement process at the pore scale level, these results are mapped into LBM simulation parameters and a microscale LBM fluid flow simulation is performed. Following the MD to LBM mapping procedure, the physical properties shown in Tab. 1 are mapped into LBM simulation parameters. The set of LBM parameters is shown in Tab. 2, which are simulated in a discrete two-dimensional lattice of the type: D_2Q_9.

Table 2: Dimensionless LBM parameters derived from the MD results show in Tab 1. The characteristic scale is: $l_o = 2.22 \times 10^{-8} m$, $t_o = 1.52 \times 10^{-10} s$ and $m_o = 9.91 \times 10^{-21} kg$

System	$\tilde{\rho}_b/\tilde{\rho}_o$	τ_b	τ_o	$\tilde{\gamma}_{bo}$	$\mathbf{g}_{bo}$	$\mathbf{g}_b^{\mathbf{MMT}}$
no-NP	1.0	1.230	4.628	0.100	0.190	-0.045
NP-H	1.0	1.299	4.513	0.089	0.181	-0.056
NP-SA	1.0	1.300	4.556	0.077	0.171	-0.058
NP-PEG2	1.0	1.288	4.546	0.068	0.164	-0.057

The LBM parameters are chosen according to the strategies and similar values described in Pereira et al., 2016, as well as through the criteria of the numbers of: Reynolds, Mach and Knudsen (Eqs. $10-12$), where: $R_e = 0.56$, $M_a = 1.27 \times 10^{-3}$ and $K_n = 2.29 \times 10^{-3}$. These criteria indicate that the flow in the simulations is: $a)$ in laminar regime ($R_e \ll 2000$), $b)$ with velocities lower than the velocity of sound ($M_a \ll 1$) and $c)$ slip flow regime close to continuous regime ($0.001 < K_n < 0.1$). Now, the PNMs have dimensions equal to 256×256 ($\tilde{L}_x \times \tilde{L}_y$) and the injection velocity is $\tilde{v} = 0.003$ in all cases, therefore, according to Eqs. $7-9$ and Tab. 2 the characteristic scales are: $l_o = 2.22 \times 10^{-8}\, m$, $t_o = 1.52 \times 10^{-10}\, s$ and $m_o = 9.91 \times 10^{-21}\, kg$.

Effect of the porous structures

To observe the effect of the structure in the EOR process, the porosity, tortuosity and the injection velocity are not modified in the simulations. Fig. 1, shows various porous structures for the EOR processes, classified into three types: $a)$ different shape, $b)$ size variation and $c)$ random distribution. For each of the cases $a)$ $b)$ or $c)$, there are four examples of porous structures. The snapshots of each of them are shown when one of them reaches 100% oil extraction.

In the first situation (Fig. 3), the extraction process of the four examples (square, hexagon, octagon and circle), follow the same pattern. No remarkable differences are observed, where, the most efficient is the square and the least efficient is the circle. The second case (Fig. 4), has four types of circle sizes: 1 very large, 4 large, 16 medium and 64 small circles. The small circles are the most efficient and the least efficient is the very large circle. Finally, in the third situation (Fig. 5), it is observed that all random distributions displace the oil by an average of 91% (oil retained approximately, 9%), even though, we double the simulation time compared to the previous two cases. Thus, in the latter case there is potential for the use of surfactants to improve the oil extraction.

Effect of the nanoparticles

To observe the importance of the surfactants, nanoparticles are added to the injected brine. In order to isolate the effects of the nanoparticle dispersed fluid injection, the porosity and the injection velocity are kept fixed. Fig. 6 shows the percentage of extracted oil for an injection time of $11.2\,\mu s$, to the four studied cases. The results show that the injection of brine without nanoparticles (no-NP) is the least efficient oil recovery process and the addition of nanoparticles increases the recovery percentage. From the three types of nanoparticles, the NP-PEG2 is the

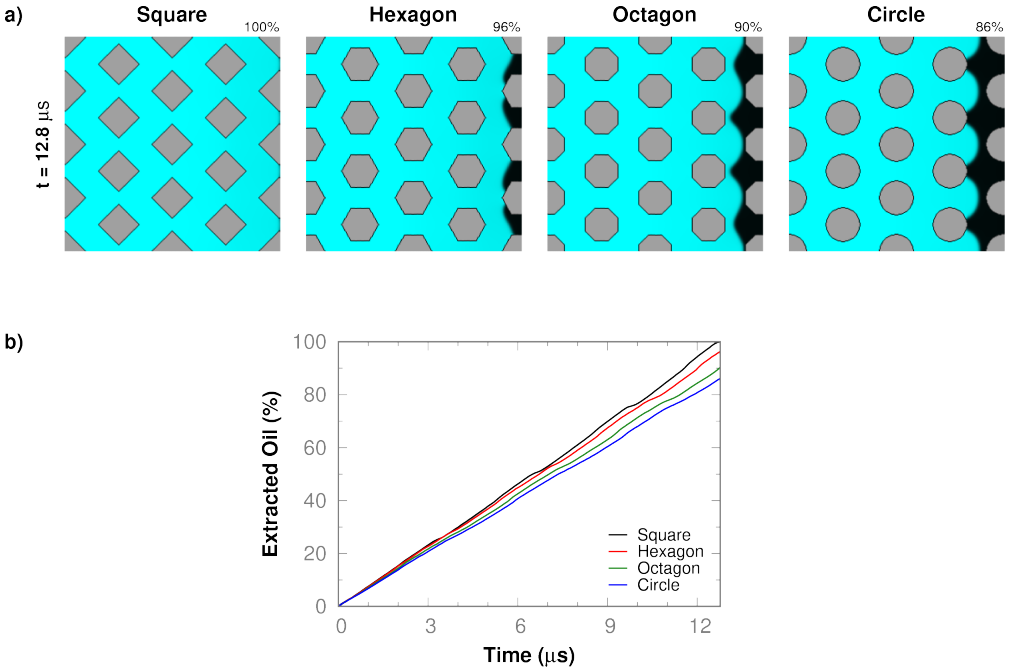

Figure 3: Oil recovery (oil: black region) from porous media of MMT (clay: gray region) as a function of injection time of API brine (brine: cyan region). a) Snapshot of oil extraction at time $12.8\,\mu s$, in porous media with pores of different shapes but the same size. b) Percentage of oil extraction, during the process of brine injection.

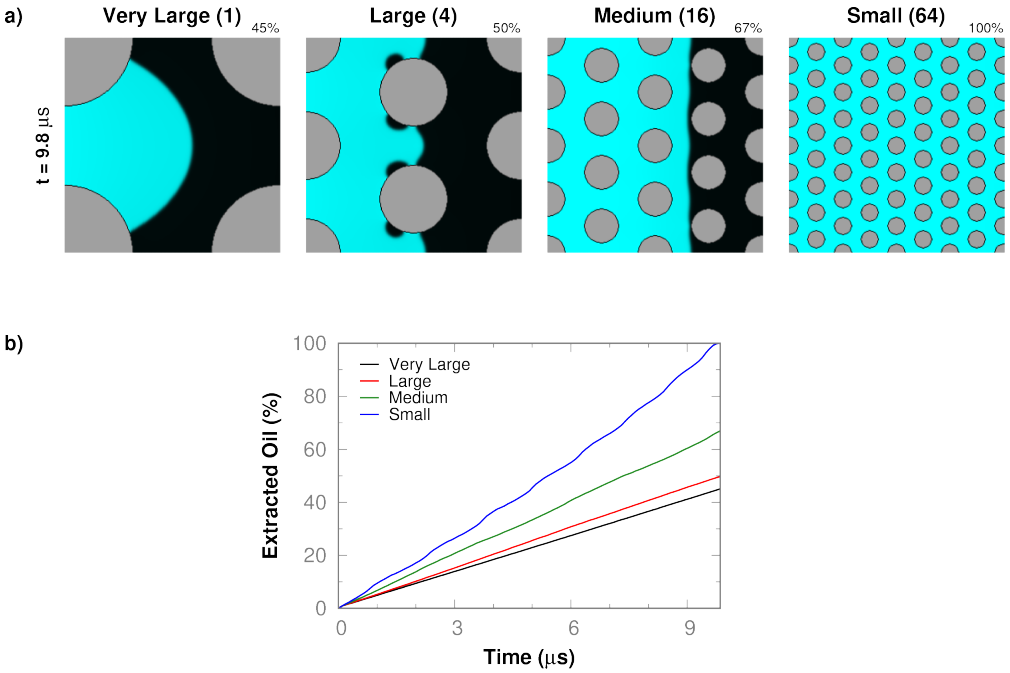

Figure 4: Oil recovery (oil: black region) from porous media of MMT (clay: gray region) as a function of injection time of the API brine (brine: cyan region). a) Snapshot of oil extraction at time $9.8\,\mu s$, in porous media with pores of different sizes with circular shapes. b) Percentage of oil extraction, during the process of brine injection.

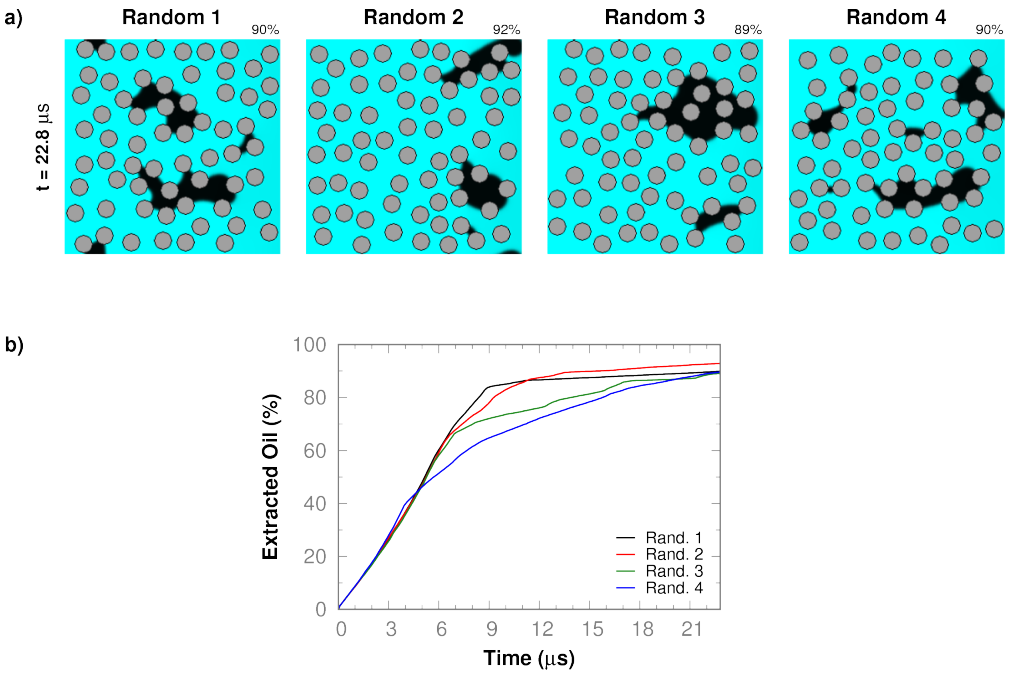

Figure 5: Oil recovery (oil: black region) from porous media of MMT (clay: gray region) as a function of injection time of API brine (brine: cyan region). a) Snapshot of oil extraction at time $22.8\,\mu s$, in porous media with small circular pores randomly distributed. b) Percentage of oil extraction during the process of brine injection, where none can extract all the oil even doubling the injection time with respect to the previous examples.

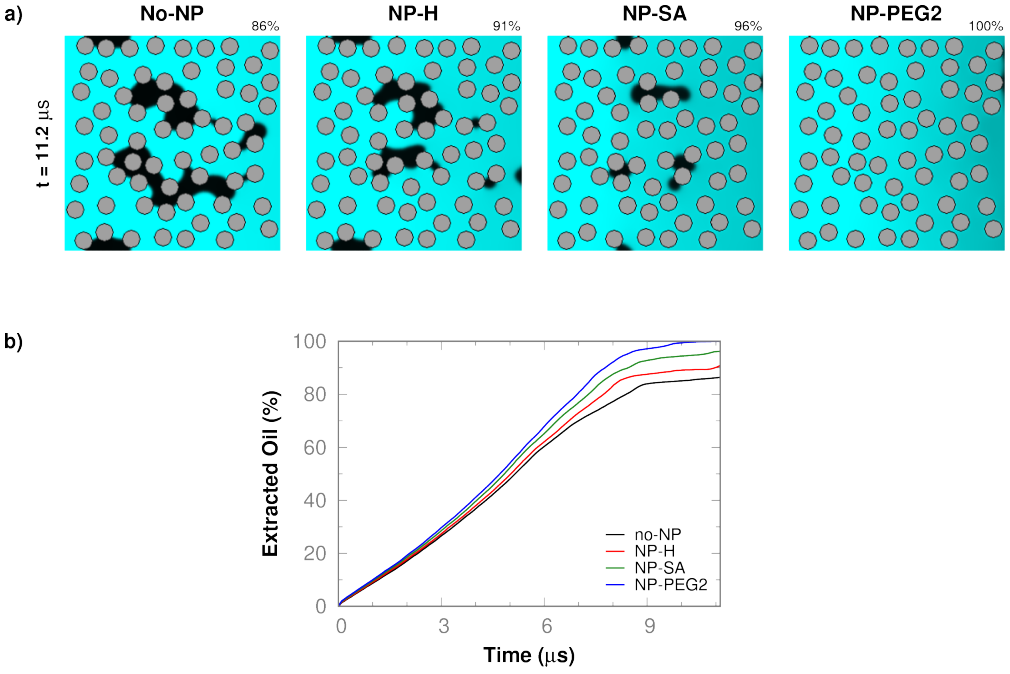

Figure 6: Oil recovery (oil: black region) from porous media of MMT (clay: gray region) as a function of injection time of API brine (brine: cyan region). a) Snapshot of oil extraction at time $11.2\,\mu s$, in the same porous media (first example of Fig. $5a$), with different injection fluids: only brine and brine plus three types of nanoparticles. b) Percentage of oil extraction, during the process of fluid injection for the four cases, where the use of nanoparticles allows to extract more oil, being the most efficient the NP-PEG2 followed by the NP-SA.

most efficient displacing 100% of oil, followed by the NP-SA that displaces 98% and finally, the least efficient is the NP-H that manages to extract 96%.

CONCLUSIONS

In this work, we apply a hierarchical multiscale computational protocol based on the combination of molecular dynamics and lattice Boltzmann method to simulate flooding injection of NPs dispersed fluids to displace oil in PNM. The oil displacement through 2D porous media was studied under different simple geometric configuration under similar porosity.

With respect to the effect of the porous structure on the amount of oil displaced, we can observe that circular porous medium are the least efficient with respect to the other forms, being the circular form the most used computationally to emulate the natural pores. For the same geometric form, the PNM formed by small circular pores is more effective with respect to the larger ones, therefore the decreasing (reduction of individual pore size but maintaining the same porosity of the system) of a porous medium, which may be related with increasing network, contributes to an increasing the EOR. For a PNM with random distribution of small circles, a given amount of oil remains trapped even after an injection of brine, which emulates better the porous network found in porous media typical of oil reservoirs. In our case, for the four randomly distributed cases studies, a retention on average 9% of oil was observed.

Finally, the effect of the NPs on the oil displacement was analysed for one of the porous media with randomly distributed pores. In this case, surfactant funtionalized nanoparticles enhanced the oil recovery within 9% compared with the brine injection. Overall, our studies shows the capability of the multiscale protocol to investigate the fluid flow throw PNM and quantify the best chemical additives (surfactants or nanoparticles) for EOR.

ACKNOWLEDGEMENTS

This project is financially support from the PETROBRAS and Brazilian agencies CNPq and FAPESP. The authors acknowledge the computational time provided by CENAPAD-SP and IFUSP SAMPA group.

REFERENCES

Morrow, N. R., 1990. Interfacial Phenomena in Petroleum Recovery. *Surfactant Science*. Taylor & Francis.

Green, D. W., Willhite, G. P., 1998. Enhanced Oil Recovery *Society of Petroleum Engineers*.

Donaldson, E. C., Alam, W., 2008. Wettability. *Gulf Publishing Company Houston, Texas*.

Starov, V. M., Velarde, M. G., Radke, C. J., 2007. Wetting and Spreading Dynamics. *CRC Press Taylor & Francis Group*.

Suleimanov B. A., Ismailov, F. S., & Veliyev, E. F., 2011. Nanofluid for enhanced oil recovery. *Journal of Petroleum Science and Engineering*, 78(2), pp. 431-437

Munshi, A. M., Singh, V. N., Kumar, Mukesh, & Singh, J. P., 2008. Effect of nanoparticle size on sessile droplet contact angle. *Journal of Applied Physics*, 103(8), p. 084315

Cygan, R. T., Liang, J. J., Kalinichev, A. G., 2004. Molecular Models of Hydroxide, Oxyhydroxide, and Clay Phases and the Development of a General Force Field. *The Journal of Physical Chemistry B*, 4(108), pp. 1255-1266

Alejandre, J., Chapela, G. A., Bresme, F., Hansen, J. P., 2009. The short range anion-H interaction is the driving force for crystal formation of ions in water. *J of Chem. Phys.*, (130), pp. 1-10

Brooks, B. R., 2009. CHARMM: the biomolecular simulation program. *J Comp. Chem.*, (30), pp. 1545-1615

Cruz-Chu, E. R., Aksimentiev, A., Schulten, K., 2006. WaterSilica Force Field for Simulating Nanodevices. *The Journal of Physical Chemistry B*, 43(110), pp. 21497-21508.

McNamara, Guy R., Zanetti, & Gianluigi, 1988. Use of the Boltzmann Equation to Simulate Lattice-Gas Automata. *Phys. Rev. Lett*, 61(20), p. 2332

Porter, M. L., Coon, E. T., Kang, Q., Moulton, J. D., & Carey, J. W., 2012. Multicomponent interparticle-potential lattice Boltzmann model for fluids with large viscosity ratios. *Phys. Rev. E*, 86(3), p 036701

Rodrigo, C. V., Coelho, Anderson, S., Ilha, Mauro, M., & Doria, 2016. A lattice Boltzmann method based on generalized polynomials and its application for electrons in metals. *EPL (Europhysics Letters)*, 116(2), p. 20001

Mendoza, M., Boghosian, B. M., Herrmann, H. J., & Succi, S., 2010. Fast Lattice Boltzmann Solver for Relativistic Hydrodynamics. *Phys. Rev. Lett*, 105(1), p. 014502

Pereira, A. O., de Lara, L. S., & Miranda, C. R., 2016. Combining molecular dynamics and lattice Boltzmann simulations: a hierarchical computational protocol for microfluidics. *Microfluidics and Nanofluidics*, 20(2), p. 36

Coon, E. T., 2014. Taxila LBM: a parallel, modular lattice Boltzmann framework for simulating pore-scale flow in porous media. *Computational Geosciences*, 18(1), pp. 17-27

Plimpton, S., 1995. Fast parallel algorithms for short-range molecular dynamics. *J Comput Phys*, (117), pp. 1-19

Miranda, C. R., de Lara, L. S., & Tonetto, B. C., 2012. Stability and mobility of functionalized silica nanoparticles for enhanced oil recovery applications. *Society Petroleum Engineering*.

de Lara, L. S., Michelon, M. F., Mateus, F., & Miranda, C. R., 2012a. Molecular Dynamics Studies of Fluid/Oil Interfaces for Improved Oil Recovery Processes. *The Journal of Physical Chemistry B*, 116(50), pp. 14667-14676

de Lara, L. S., Michelon, M. F., Metin, C. O., Nguyen, Q. P., & Miranda, C. R., 2012b. Interface tension of silica hydroxylated nanoparticle with brine: A combined experimental and molecular dynamics study. *The Journal of Chemical Physics*, 136(16), p. 164702

Rigo, V. A., de Lara, L. S., & Miranda, C. R., 2014. Energetics of formation and hydration of functionalized silica nanoparticles: an atomistic computational study. *Applied Surface Science*, 292, pp. 742-749

Sánchez, V. M., & Miranda, C. R., 2014. Modeling Acid Oil Component Interactions with Carbonate Reservoirs: A First-Principles View on Low Salinity Recovery Mechanisms. *The Journal of Physical Chemistry C*, 118(33), pp. 19180-19187

Alvim, R. S., Suxo, V. M., Babilonia, O. A., Celaschi, Y. M., & Miranda, C. R., 2017. Nanoscience Applied to Oil Recovery and Mitigation: A Multiscale Computational Approach. *MRS Advances*, 2(9), pp. 477-482

Sukop, M. C., & Thorne, D. T., 2007. Lattice Boltzmann Modeling: An Introduction for Geoscientists and Engineers. *Springer*.

Succi, S., 2001. The Lattice Boltzmann Equation for Fluid Dynamics and Beyond. *Oxford university press*.

Mohamad, A. A., 2011. Lattice Boltzmann Method: Fundamentals and Engineering Applications with Computer Codes. *Springer Science & Business*.

Yang, F., Shi, X., Guo, X., Sai, Q., 2012. MRT Lattice Boltzmann Schemes for High Reynolds Number Flow in Two-Dimensional Lid-Driven Semi-Circular Cavity. *Energy Procedia*, (16), pp. 639-644

Gan, Y., Xu, A., Zhang, G., Yu, X., Li, Y., 2008. Two-dimensional lattice Boltzmann model for compressible flows with high Mach number. *Physica A: Statistical Mechanics and its Applications*, 8(387), pp. 1721-1732

Inamuro, T., Yoshino, M., Ogino, F., 1997. Accuracy of the lattice Boltzmann method for small Knudsen number with finite Reynolds number. *Physics of Fluids*, 9(11), pp. 3535-3542

Scheidegger, A. E., 1974. The physics of flow through porous media. *University of Toronto Press: London*.

Duda, A., Koza, Zbigniew, Matyka, & Maciej, 2011. Hydraulic tortuosity in arbitrary porous media flow. *Phys. Rev. E*, 84(3), p. 036319